BMC Cancer

RESEARCH

Open Access

# NDRG1 alleviates Erastin-induced ferroptosis of hepatocellular carcinoma

Liuzheng Li[1], Tong Wu[1*], Guocha Gong[1], Bo Li[1], Jiawei Feng[1], Leisheng Xu[1], Hairong Zhao[1] and Xuechang Gao[1]

## Abstract

**Background** NDRG1, a cell differentiation-associated factor, has recently emerged as a regulator ferroptosis. Nevertheless, its role in modulating ferroptosis within hepatocellular carcinoma (HCC) remains uncharacterized.

**Methods** The differential expression of NDRG1 and its prognostic value were analyzed in HCC using data from TCGA and GEO. Ferroptosis in HepG2 and Huh7 cells was assessed using flow cytometry, transmission electron microscopy, and propidium iodide staining following NDRG1 knockdown using shRNA. RNA-seq was performed to characterize the mRNA expression profiles in HepG2 cells, identifying differentially expressed mRNAs (DE-mRNAs) and NDRG1-related hub genes.

**Results** NDRG1 was overexpressed in multiple malignant tumors, including HCC, and was associated with a significantly poor prognosis in HCC patients. A nomogram model integrating NDRG1 expression and clinical parameters demonstrated robust prognostic accuracy. NDRG1 knockdown potentiated erastin-induced alterations in $Fe^{2+}$, total ROS, lipid ROS, and ferroptosis markers (PTGS2, ACSL4, GPX4, SLC7A11, GSH, GSSG), while exacerbating mitochondrial ultrastructural damage in HepG2 and Huh7 cells. Erastin induction elicited 1,056 DE-mRNAs, while subsequent NDRG1 knockdown revealed 1,323 DE-mRNAs in HepG2 cells. These DE-mRNAs are mainly involved in metastasis, immunity, growth, ferroptosis, and are associated with AMPK, MAPK, and PI3K/AKT pathways. Moreover, NDRG1 potentially interacted with HSPA8, CDH1, ALDOC, ANGPTL4, ANKRD37, CA9, ERBB3, FOS. qRT-PCR confirmed their expression changes consistent with RNA-seq.

**Conclusion** NDRG1 exhibits strong predictive value for HCC, and accelerates tumor progression by suppressing ferroptosis.

**Keywords** Hepatocellular carcinoma, Ferroptosis, Bioinformatics, RNA sequencing, N-myc downstream regulated gene-1

*Correspondence:
Tong Wu
15769957528@163.com
[1]Hepatobiliary Surgery, The People's Hospital of Lincang, No.116 Nantang Street, Lincang, Yunnan 677000, China

## Introduction

Primary liver cancer (PLC) accounted for 8.3% of cancer-related deaths and 4.7% of the global incidence of all tumor types, making it the third leading cause of cancer mortality worldwide [1]. Hepatocellular carcinoma (HCC) accounts for 90% of PLC cases, with treatment options including surgical resection, liver transplantation, transhepatic arterial chemoembolization (TACE), radiation therapy, and first- or second-line chemotherapy [2, 3]. Although various therapeutic strategies can improve patient survival, challenges such as high recurrence rate, complications, controversial efficacy, and drug resistance [2, 3]. Therefore, further investigation into the molecular pathogenesis of HCC is urgently needed, along with the identification of biomarkers for early diagnosis and targeted therapies.

N-myc downstream regulated gene-1 (NDRG1) belongs to the NDRG family, a group of genes recently identified as being involved in cell differentiation. NDRG1 has been shown to play diverse roles in breast, colorectal, gastric, and prostate cancers, including the regulation of proliferation, metastasis, angiogenesis, and sensitivity to radiotherapy and chemotherapy [4–6]. In HCC, NDRG1 is considered as a cancer-promoting factor [7, 8]. Recent studies suggest that NDRG1 mediates ferroptosis, and two bioinformatics analyses have identified NDRG1 as a ferroptosis- and immune-related biomarker for HCC prognosis [9, 10]. Ferroptosis is a distinct form of programmed cell death, independent of apoptosis and autophagy, characterized by the accumulation of intracellular ferrous ions and lipid peroxidation [11, 12]. Ferroptosis has been demonstrated to interact with autophagy, tumor immune microenvironment, and tumor stem cell stemness, thereby altering the sensitivity of HCC cells to chemotherapy [13–15]. Consequently, lipid peroxidation- and ferrous ion-dependent ferroptosis is emerging as a promising therapeutic target in tumor therapy. Nevertheless, it remains unclear whether NDRG1 regulates the ferroptosis process in HCC and its underlying molecular mechanisms.

The present study intends to identify the differential expression and prognostic value of NDRG1 in HCC using bioinformatics, and to investigate the function of NDRG1 in the ferroptosis process through in vitro experiments. Additionally, the potential molecular mechanism underlying NDRG1-mediated ferroptosis in HCC cells was characterized using RNA-seq, providing insights for the development of therapeutic strategies for HCC.

## Materials and methods

### NDRG1-related bioinformatics analyses

Pan-cancer differences in NDRG1 expression and its correlation with the prognosis of HCC patients were analyzed using bioinformatics. Pan-cancer differences in NDRG1 expression were assessed using the GENT2 [16] and GEPIA2 [17] web. GENT2 includes data from the GPL96 and GPL570 platforms, while GEPIA2 provides data from the TCGA database. The correlation between NDRG1 expression and the prognosis of HCC patients was performed using the TCGA-LIHC dataset, which includes the expression profiles and clinical characteristics of 374 patients. A log-rank test and Cox regression analysis were performed on the TCGA-LIHC dataset to assess the correlation between NDRG1 expression, clinical features, and prognosis in HCC patients, using the survival package in R software [18]. Visualization was performed using the survminer package in R. The rms package [19] in R was used for the construction and calibration analysis of nomogram models based on NDRG1 expression and clinical features.

### Immunohistochemical staining of HCC tissues

In this study, 12 pairs of HCC and adjacent cancer tissues, obtained from patients who underwent surgical resection, were collected for immunohistochemical (IHC) staining to validate the differences in NDRG1 expression. Briefly, sodium citrate antigen retrieval solution (Beyotime, CHN), 3% hydrogen peroxide (MCE, USA), and goat serum sealing solution (Thermo Fisher, USA) were applied for antigen retrieval, endogenous enzyme inactivation, and blocking of nonspecific binding sites in paraffin-embedded HCC and adjacent tissues, respectively. Paraffin sections were incubated with NDRG1 rabbit mAb (1:300; Abcam, USA) and enhanced enzyme-labeled goat anti-mouse/rabbit IgG polymer (ZSGB-BIO, CHN). DAB kit (Beyotime) and hematoxylin (Beyotime) were used for color development and nuclei counterstaining, respectively. The sections were scanned using an EasyScan 60 scanner (Motic, Hong Kong, CHN).

### HCC cell culture and transfection

Cell subjects for this study included LO2 (BNCC338358), HepG2 (BNCC338070), Huh7 (BNCC337690), MHCC97H (BNCC359345), and PLC/PRF/5 (BNCC340696) cells, were purchased from the BeNa Culture Collection. The culture medium for all cells consisted of DMEM supplemented with 1% penicillin-Streptomycin and 10% FBS, and cells were maintained at 37 °C with 5% $CO_2$. Short hairpin RNA (shRNA) targeting NDRG1 (sh-NDRG1) and its negative control were synthesized by RIBOBIO (Guangzhou, CHN), and cloned into the pRNAT-U6.1/Neo vector. HepG2 and Huh7 cells were randomly assigned to the Control, Erastin, KD-NC and KD-NDRG1 groups. HepG2 and Huh7 cells in the Erastin, KD-NC and KD-NDRG1 groups were treated with 10 μM Erastin (MCE) for 24 h, as previously described [20]. HepG2 and Huh7 cells in the KD-NDRG1 and KD-NC groups were transfected with sh-NDRG1

and its negative control vector, respectively, using Lipofectamine 3000 (Invitrogen, USA).

#### HCC cell viability and death assays

Cell viability and death assays were performed using a CCK-8 kit and propidium iodide (PI) solution, respectively. For CCK-8 assay, HepG2 and Huh7 cells (5 × 105 cells/mL) were seeded into 96-well plates at 100 µL per well, and cultured for 12, 24, 36 and 48 h. Each well of HepG2 and Huh7 cells was treated with 10 µL of CCK-8 solution (Biosharp, CHN), and the optical density was measured at 450 nm using a Multiskan SkyHigh spectrophotometer (Thermo Fisher). For PI staining, HepG2 and Huh7 cells were fixed with acetone and stained with 200 µL PI Solution (Solarbio, USA) for 15 min. Bright field and fluorescence images were captured using an IX73 inverted microscope (Olympus, Japan).

#### Ferroptosis-associated flow cytometry

The levels of $^{F2+}$, total ROS, and lipid ROS were assayed using Phen Green SK diacetate (PGSK; MCE), Reactive Oxygen Species Assay Kit (Beyotime), and BODIPY™ 581/591 C11 (Invitrogen), respectively. Briefly, HepG2 and Huh7 cells were incubated with fluorescent probes at final concentrations of 20 µM PGSK, 100 µM DCFH-DA, and 50 µM C11-BODIPY. After a 20-minute incubation, the percentage of positive cells for PGSK, DCF, and C11-BODIPY were measured using NovoCyte Penteon flow cytometry (Agilent, USA).

#### Detection of markers involved in ferroptosis

Western blotting and RT-qPCR were applied to measure the protein and mRNA expression of ferroptosis-related markers (PTGS2, ACSL4, GPX4, and SLC7A11) in each group of HepG2 and Huh7 cells. Antibody information for the target protein is provided in Supplementary Table (1) The primer sequences for NDRG1 were: CTGTCAT CCTCACCTACC (F) and ATGTCCTCGTAGTTGAAG A (R). The primer sequences for GAPDH were: TTGCC CTCAACGACCACTTT (F) and TGGTCCAGGGGTC TTACTCC (R). The primer sequences for the hub genes are provided in Supplementary Table (2) The levels of GSH and GSSG in HepG2 and Huh7 cells were measured following the protocols outlined in the Reduced Glutathione (GSH) Content Assay Kit and Oxidized Glutathione (GSSG) Content Assay Kit (Solarbio). Absorbance was recorded at 412 nm using the Multiskan SkyHigh spectrophotometer.

#### NDRG1-related RNA-seq

Total RNA extraction, RNA quality control, library construction, and RNA-seq for were performed for the Control, Erastin and KD-NDRG1 groups of HepG2 cells (three replicates per group, 9 samples in total) by oebiotech (Shanghai, CHN) using TRIzol reagent (Thermo Fisher), the Agilent 2100 Bioanalyzer (Agilent, USA), the VAHTS Universal V5 RNA-seq Library Prep kit (Vazyme, China), and the Novaseq 6000 (llumina, USA). The nine samples generated a total of 62.41 G of clean data with an average GC content of 52.75%. After mapping the clean data to the GRCh38.p13 reference genome, the comparison rate of expression profiles was 97.82–98.39%.

For bioinformatics analysis, the DESeq2 package [21] in R software was used to normalize gene counts and calculate the folds change (FC), followed by significance testing using the negative binomial distribution test to identify differentially expressed mRNAs (DE-mRNAs). The DE-mRNAs screening threshold is adjusted $P < 0.05$ and $|\log_2 FC| > 1$. GO and KEGG enrichment analysis was performed using the clusterProfiler package [22] in R software. The results were visualized using the ggplot2 package [23] in R software. DE-mRNAs were used to predict interactions via the String database [24], and protein-protein interaction (PPI) networks were visualized in Cytoscape software [25].

#### Statistical analysis

Statistical analysis and visualization were performed using GraphPad prism software (Graph Pad Inc., USA), with data presented as mean ± S.E. Statistical analysis of the optical density of HCC and adjacent cancer tissues was conducted using paired *t*-test. Comparisons between multiple groups were made using one-way ANOVA followed by Tukey HSD test or Kruskal-Wallis test, with *P* values < 0.05 considered statistically different.

## Results

#### Overexpression of NDRG1 is associated with poor prognosis in HCC patients

To investigate the altered expression of NDRG1 in HCC, this study analyzed microarray (GPL96 and GPL570 platforms) and sequencing (TCGA) datasets. The differences in NDRG1 expression across these datasets were largely consistent, with NDRG1 being overexpressed in multiple malignant tumors, except for ACC, SKCM, TGCT, and THCA (Fig. 1A and C). Notably, NDRG1 was significantly overexpressed in HCC tissues from the GPL96, GPL570 and TCGA datasets (Fig. 1A and C). HPA database further corroborated these findings, showing elevated NDRG1 protein levels in HCC tissues compared to normal liver tissues (Fig. 1D). IHC confirmed a significant increase in the optical density of NDRG1 in HCC tissues compared to adjacent tissues (Fig. 1E).

Given the aberrant expression of NDRG1, this study next examined its relationship between with the prognosis of HCC patients. High expression of NDRG1 was associated with advanced tumor and T-stage (Table 1).

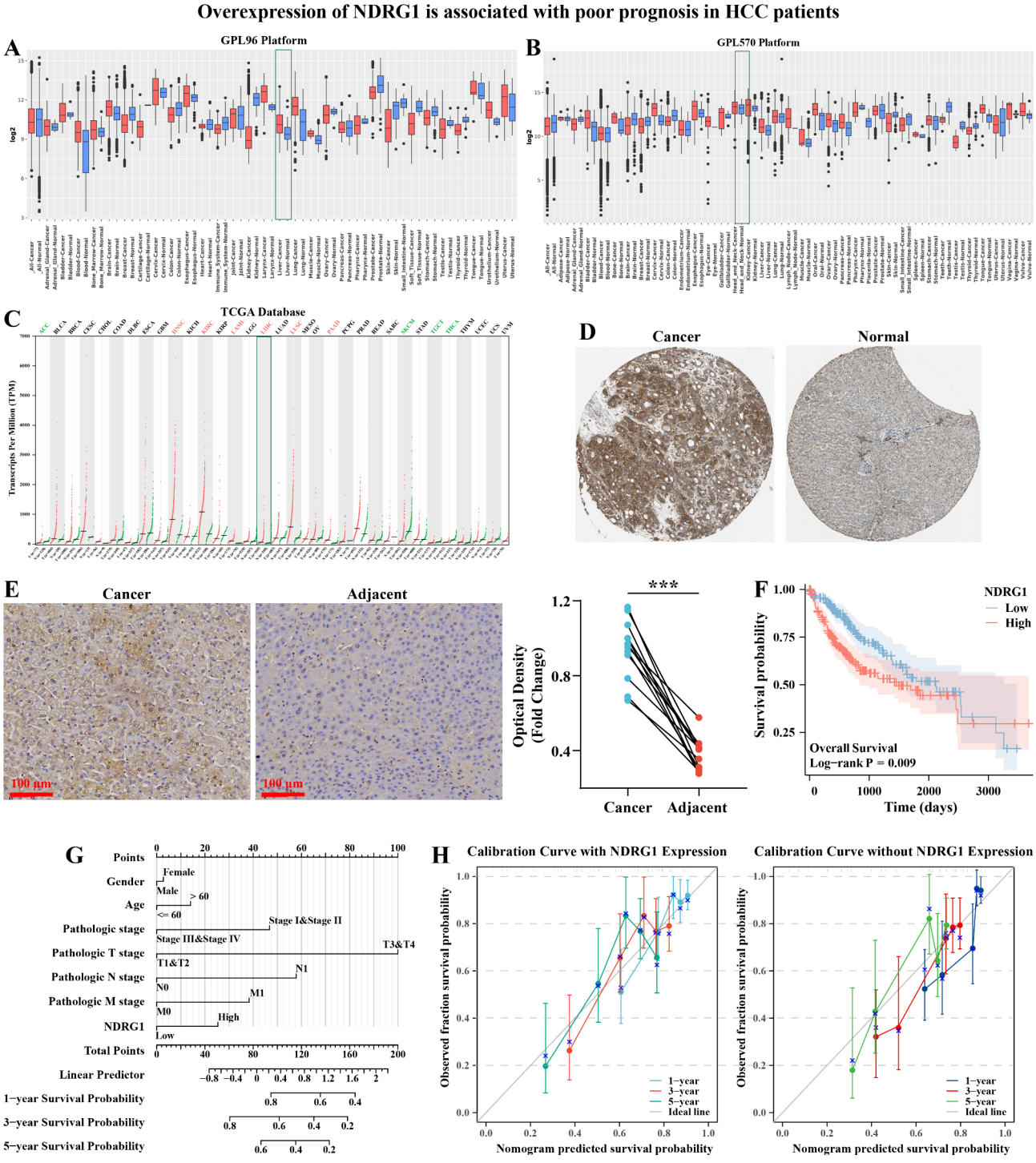


**Fig. 1** Overexpression of NDRG1 is associated with poor prognosis in HCC patients. **A-B**: Pan-cancer expression of NDRG1 was analyzed in the GPL96 **(A)** and GPL570 **(B)** platform datasets from the GEO database using the GENT2 Web. The red and blue columns represent tumor and normal tissue samples, respectively, for comparison. **C**: Differential pan-cancer expression of NDRG1 in the TCGA dataset was analyzed using the GEPIA2. Red and green fonts denote high and low expression of NDRG1 in corresponding malignant tumors, respectively, indicating statistical significance. **D**: Representative IHC images of NDRG1 expression in HCC and normal liver tissues were obtained from the HPA database. **E**: Differential expression of NDRG1 protein in HCC and adjacent cancer tissues was evaluated by IHC staining. Compared to the Adjacent group, $^{***}P < 0.001$. **F**: The median value of NDRG1 expression in the TCGA-LIHC dataset was used as a cutoff value to stratify the cohort into high and low NDRG1 expression groups. The difference in overall survival between the two groups was analyzed using the log-rank test. **G**: A nomogram model was constructed based on NDRG1 expression and clinical characteristics, including gender, age, stage, T stage, N stage, and M stage. **H**: Calibration curves with NDRG1 expression and without NDRG1 expression were used to assess the predictive performance of the nomograms for survival probability in HCC patients at first, second and third years

**Table 1** NDRG1 expression-related baseline information table

| Characteristics | NDRG1 Low expression (*n* = 187) | NDRG1 High expression (*n* = 187) | *P* value |
|---|---|---|---|
| **Gender, n (%)** | | | 0.581 |
| Female | 58 (15.5%) | 63 (16.8%) | |
| Male | 129 (34.5%) | 124 (33.2%) | |
| **Age, n (%)** | | | 0.055 |
| <= 60 | 79 (21.2%) | 98 (26.3%) | |
| > 60 | 107 (28.7%) | 89 (23.9%) | |
| **Stage, n (%)** | | | **0.004** |
| I & II | 141 (40.3%) | 119 (34%) | |
| IV & III | 33 (9.4%) | 57 (16.3%) | |
| **T stage, n (%)** | | | **0.004** |
| T1 &T2 | 150 (40.4%) | 128 (34.5%) | |
| T3 &T4 | 34 (9.2%) | 59 (15.9%) | |
| **N stage, n (%)** | | | 0.625 |
| N0 | 127 (49.2%) | 127 (49.2%) | |
| N1 | 1 (0.4%) | 3 (1.2%) | |
| **M stage, n (%)** | | | 1.000 |
| M0 | 130 (47.8%) | 138 (50.7%) | |
| M1 | 2 (0.7%) | 2 (0.7%) | |

High expression of NDRG1 significantly correlated with poorer prognosis in HCC patients, as confirmed by both log-rank and univariate Cox analysis (Fig. 1F; Table 2). Moreover, based on multivariate Cox analysis, this study constructed a nomogram model incorporating gender, age, tumor stage, T-stage, N-stage, M-stage, and NDRG1 expression (Fig. 1G). Calibration curves validated the predictive accuracy of the NDRG1-associated nomogram model for HCC patient survival in the first, second, and third years (Fig. 1H). Notably, the survival of HCC patients predicted by a nomogram model incorporating NDRG1 expression more accurately reflects observed outcomes compared to a model that excludes NDRG1 expression. These findings suggest that NDRG1 is associated with poor prognosis in HCC patients.

### NDRG1 alleviates ferroptosis in HCC cells

NDRG1 has been proven to mediate iron metabolism [26] and is associated with ferroptosis [9, 10]. Therefore, this study further investigates the role of NDRG1 in ferroptosis in HCC. Similar to HCC tissues, NDRG1 was overexpressed in HCC cells, with both NDRG1 mRNA and protein being higher in HepG2 and Huh7 cells (Fig. 2A and B). NDRG1 expression was significantly reduced following transfection with sh-NDRG1, with construct #1 being most effective in HepG2 cells and #3 in Huh7 cells (Fig. 2C and F), which were selected for subsequent experiments. Notably, treatment with erastin (ferroptosis inducer) resulted in reduced NDRG1 protein levels in HepG2 and Huh7 cells, and sh-NDRG1 transfection further decreased NDRG1 expression (Fig. 3A).

Functional assays demonstrated that erastin treatment decreased the viability of HepG2 and Huh7 cells from 24 h onwards, and sh-NDRG1 transfection further

**Table 2** Univariate and multivariate COX analysis for the association of NDRG1 expression and clinical characteristics with the prognosis of HCC patients

| Characteristics | | Univariate analysis | | Multivariate analysis | |
|---|---|---|---|---|---|
| | Total (*N*) | HR (95% CI) | *P* value | HR (95% CI) | *P* value |
| **Gender** | 373 | | | | |
| Female | 121 | 0.79 (0.56–1.13) | **0.200** | | |
| Male | 252 | | | | |
| **Age** | 373 | | | | |
| <= 60 | 177 | 1.21 (0.85–1.71) | **0.295** | | |
| > 60 | 196 | | | | |
| **Stage** | 349 | | | | |
| I & II | 259 | 2.50 (1.73–3.63) | **< 0.001** | 1.28 (0.18–9.32) | 0.807 |
| III & IV | 90 | | | | |
| **T stage** | 370 | | | | |
| T1 & T2 | 277 | 2.60 (1.83–3.70) | **< 0.001** | 1.93 (0.26–14.14) | 0.517 |
| T3 & T4 | 93 | | | | |
| **N stage** | 258 | | | | |
| N0 | 254 | 2.03 (0.50–8.28) | 0.324 | | |
| N1 | 4 | | | | |
| **M stage** | 272 | | | | |
| M0 | 268 | 4.08 (1.28–12.97) | **0.017** | | |
| M1 | 4 | | | | |
| **NDRG1** | 373 | | | | |
| Low | 186 | 1.58 (1.12–2.24) | **0.010** | 1.44 (0.99–2.08) | 0.055 |
| High | 187 | | | | |

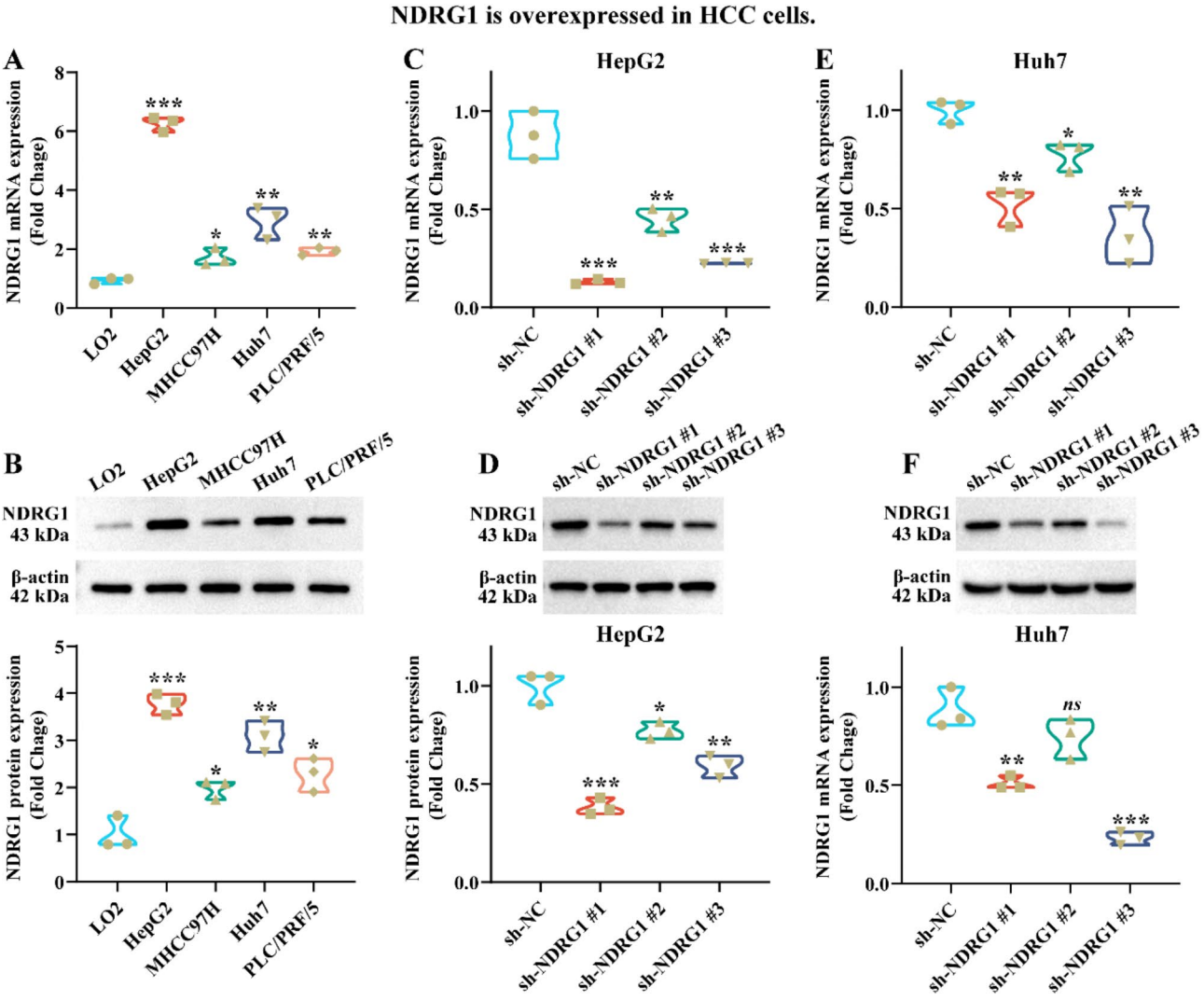


**Fig. 2** NDRG1 is overexpressed in HCC cells. **A-B**: Differential expression of NDRG1 mRNA and protein in human normal hepatocytes (LO2) and HCC cells (HepG2, MHCC97H, Huh7, and PLC/PRF/5) were assessed by RT-qPCR **(A)** and western blotting **(B)**. **C-D**: Effect of sh-NDRG1 transfection on NDRG1 mRNA **(C)** and protein **(D)** expression in HepG2 cells was evaluated. **E-F**: Expression of NDRG1 mRNA **(E)** and protein **(F)** in Huh7 cells following transfection with sh-NDRG1. Compared to the LO2 or sh-NC groups, $^{*}P<0.05$, $^{**}P<0.01$, and $^{***}P<0.001$

inhibited cell viability (Fig. 3B). PI staining revealed that NDRG1 knockdown exacerbated erastin-induced cell death in HepG2 and Huh7 cells (Fig. 3C). Compared to the Control group, mitochondria in the Erastin and KD-NC groups displayed reduced or lost internal cristae, a phenomenon more pronounced in the KD-NDRG1 group, which exhibited near-complete loss of intact mitochondrial structures (Fig. 3D). Flow cytometry revealed that erastin treatment increased levels of Fe2+, ROS, and lipid-ROS in HepG2 and Huh7 cells, with this effect being more pronounced in those with NDRG1 knockdown (Fig. 4A and C). Additionally, this study evaluated the effect of NDRG1 on ferroptosis-related markers (PTGS2, ACSL4, GPX4, and SLC7A11). Previous studies have revealed that increased expression of PTGS2 and ACSL4 and decreased GPX4 and SLC7A11 are associated with the development of ferroptosis [27]. As illustrated in Fig. 5A and B, erastin enhanced the expression of PTGS2 and ACSL4, and diminished expression of GPX4 and SLC7A11 in HepG2 and Huh7 cells. NDRG1 knockdown exacerbated these changes in marker expression. The changes in these markers are consistent with an inhibitory effect of NDRG1 on ferroptosis. Moreover, NDRG1 knockdown further exacerbated erastin-induced reductions of GSH and GSSG levels in HepG2 and Huh7 cells (Fig. 5C and D). These findings suggest that NDRG1 alleviates ferroptosis, thereby promoting progression of HCC.

### Identification of DE-mRNAs in HCC

To elucidate the molecular mechanism underlying NDRG1-mediated ferroptosis in HCC, RNA-seq was

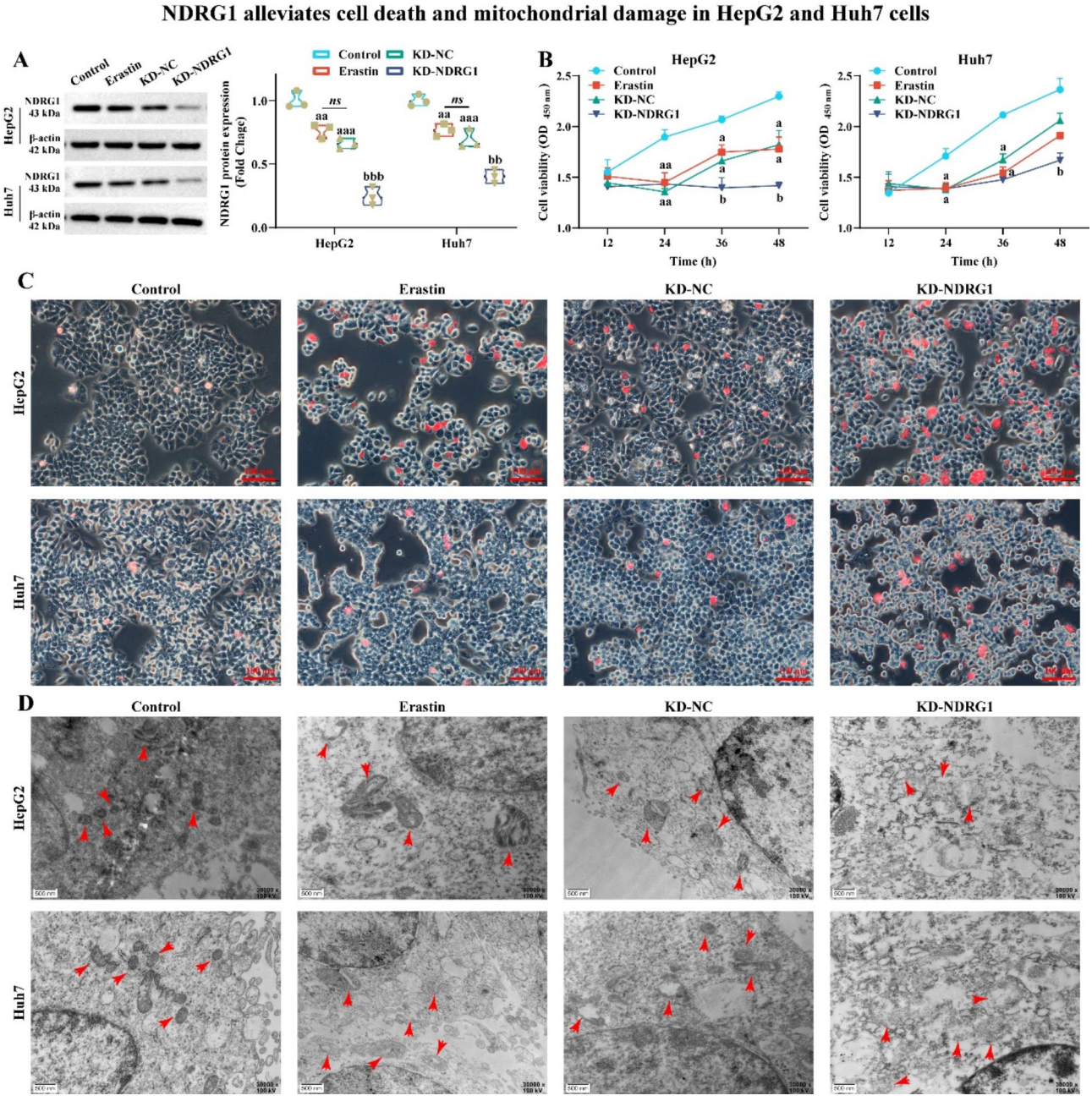


**Fig. 3** NDRG1 alleviates cell death and mitochondrial damage in HepG2 and Huh7 cells. **A**: Representative images of NDRG1 gel blot and statistical analysis of NDRG1 expression in HepG2 and Huh7 cells across different group. **B**: Cell viability of HepG2 (left) and Huh7 (right) cells was assessed at 12, 24, 36, and 48 h in each group. **C**: Representative images of PI staining and bright-field microscopy of HepG2 (top) and Huh7 (bottom) cells in each group. Red staining indicates PI-positive cells, representing dead cells. **D**: TEM was used to observe the effect of NDRG1 on mitochondrial damage in HepG2 (top) and Huh7 (bottom) cells. The red arrow indicates mitochondria. Compared to the Control group, $^{a}P<0.05$ and $^{aa}P<0.01$; Compared to the KD-NC group, $^{b}P<0.05$, $^{bb}P<0.01$, and $^{bbb}P<0.001$

conducted on HepG2 cells. Following normalization, the median values of the PKM were nearly identical across the samples, indicating a comparable degree of dispersion in the expression profile (Fig. 6A). Principal component analysis (PCA) revealed clustering of samples within each group and greater dispersion between groups, indicating that the expression profiles were similar within groups and distinct between groups (Fig. 6B). The sample distances calculated using the Euclidean algorithm further supported this observation (Fig. 6C). Compared to the Control group, the Erastin group exhibited 217 significantly up-regulated and 839 significantly down-regulated DE-mRNAs in the Erastin group, totaling 1,056 DE-mRNAs (Fig. 6D, adjusted $P<0.05$ and $|\log_2 FC|>1$).

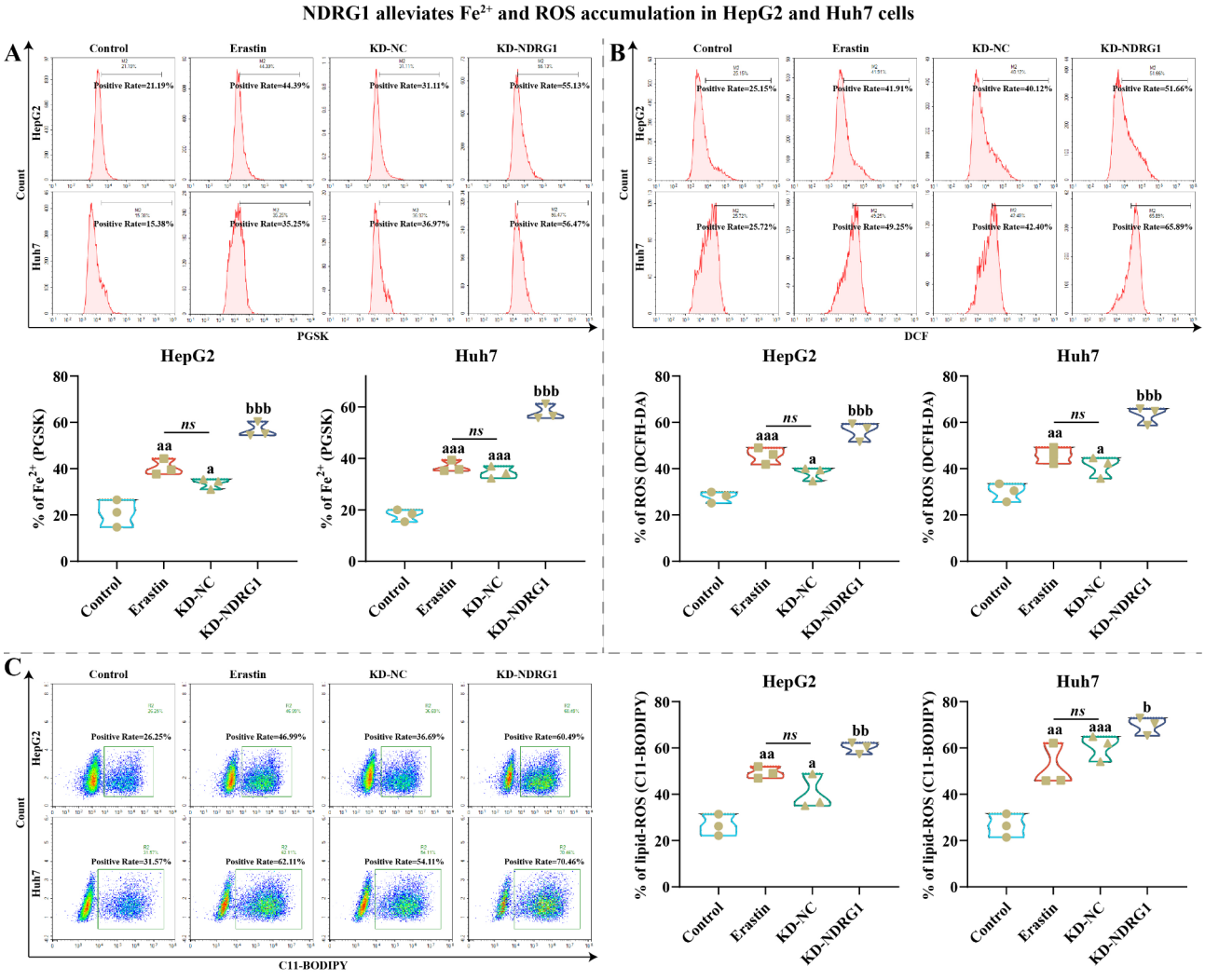


**Fig. 4** NDRG1 alleviates $Fe^{2+}$ and ROS accumulation in HepG2 and Huh7 cells. **A-C**: Phen Green SK diacetate (5/6-mixture), Reactive Oxygen Species Assay Kit, and BODIPY™ 581/591 C11 were used to detect the changes in $Fe^{2+}$ **(A)**, total ROS **(B)**, and lipid ROS **(C)** levels in HepG2 and Huh7 cells using flow cytometry. Compared to the Control group, $^{a}P<0.05$ and $^{aa}P<0.01$, and $^{aaa}P<0.001$; Compared to the KD-NC group, $^{b}P<0.05$, $^{bb}P<0.01$, and $^{bbb}P<0.001$

The expression profiles of DE-mRNAs are shown in Fig. 6E, with RPS4Y1, UCHL1, KCNQ3, MACROH2A2, and EMB representing the top five ranked DE-mRNAs by$|\log_2 FC|$ (Fig. 6F). Moreover, there were 1,323 DE-mRNAs in the Sh-NDRG1 group compared to the Erastin group (Fig. 6G), with the top five$|\log_2 FC|$ DE-mRNAs being EGR1, TNNT1, EXD3, ERBB3 and TXNOP (Fig. 6H-I). These findings suggest that these DE-mRNAs may represent potential mediators of NDRG1-mediated ferroptosis in HCC.

### Enrichment analysis of DE-mRNAs

To gain insight into the functions and related pathways involved of these DE-mRNAs in organisms, an enrichment analysis was performed. GO enrichment revealed that DE-mRNAs in Erastin vs. Control were predominantly membrane proteins and extracellular matrix (ECM), involved in regulating processes such as metastasis, immunity, growth, and calcium ion transport (Fig. 7A and Supplemental File 1, adjusted $P<0.05$). The cellular components of DE-mRNAs in Sh-NDRG1 vs. Erastin were mainly ECM, vesicular proteins, and chemokines, functioning similarly to DE-mRNAs in Erastin vs. Control (Fig. 7B and Supplemental File 1, adjusted $P<0.05$). KEGG enrichment analysis displayed that DE-mRNAs in Erastin vs. Control mainly regulate pathways such as ErbB, cAMP, AMPK, MAPK, and PI3K/AKT (Fig. 7C and Supplemental File 2, adjusted $P<0.05$). DE-mRNAs in Sh-NDRG1 vs. Erastin are implicated in regulatory pathways related to ferroptosis, endocytosis, immunity, metastasis, and ECM (Fig. 7D and Supplemental File 2, adjusted $P<0.05$).

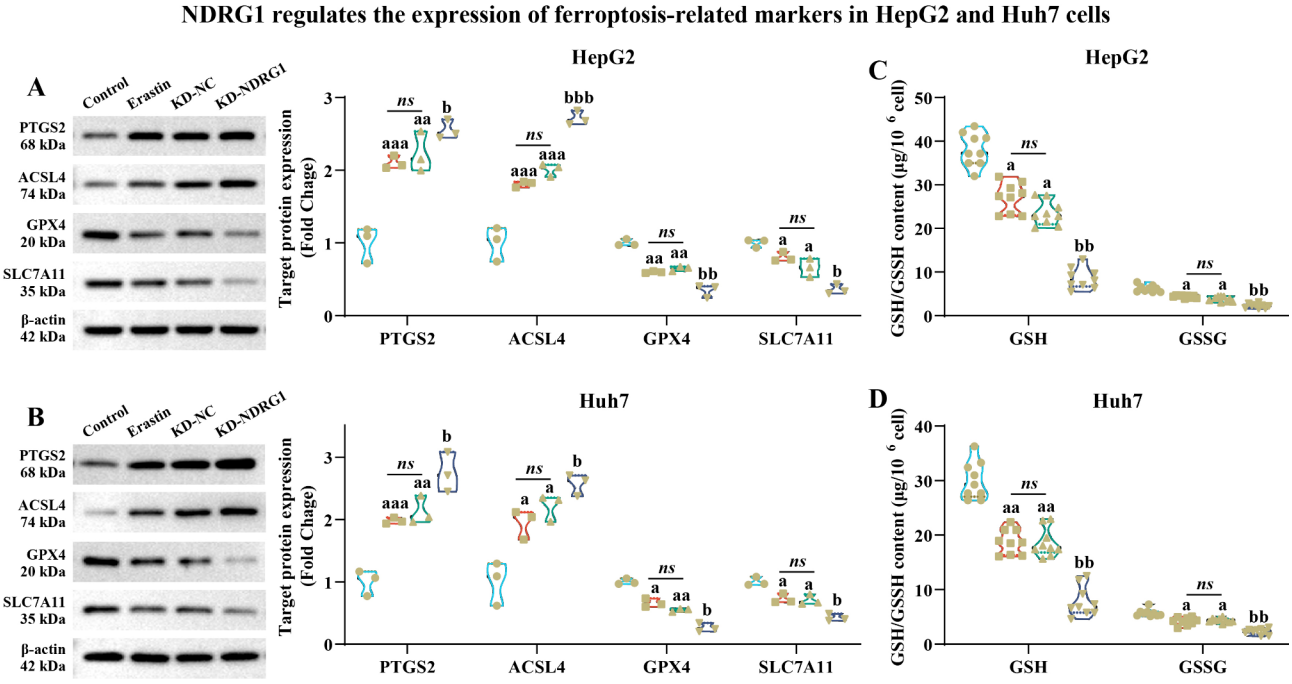


**Fig. 5** NDRG1 regulates the expression of ferroptosis-related markers in HepG2 and Huh7 cells. **A-B**: Changes in the expression of ferroptosis-related markers (PTGS2, ACSL4, GPX4, and SLC7A11) in HepG2 **(A)** and Huh7 **(B)** cells from each group were assessed by Western blotting. **C-D**: ELISA assays were used to determine the effect of NDRG1 on GSH and GSSG levels in HepG2 **(C)** and Huh7 **(D)** cells. Compared to the Control group, $^{a}P<0.05$ and $^{aa}P<0.01$, and $^{aaa}P<0.001$; Compared to the KD-NC group, $^{b}P<0.05$, $^{bb}P<0.01$, and $^{bbb}P<0.001$

### Identification of hub genes for DE-mRNAs

Further, this study constructed a PPI network using the String database to identify hub genes among the DE-mRNAs. The PPI networks of DE-mRNAs, showing the top 30 relationships, are presented in Fig. 8A and B. FOS, PIK3CD, NEURL1B, VWF, HSFA8, DNAJA1, PNO1, and HSPH1 represent the hub genes with the largest degree in the network (Fig. 8A and B). To further hub genes associated with NDRG1 and ferroptosis, this study identified common DE-mRNAs in Erastin vs. Control and Sh-NDRG1 vs. Erastin, and constructed a PPI network using these common DE-mRNAs. A total of 718 DE-mRNAs were identified (Fig. 8C), and the PPI network contained 362 nodes and 889 edges (Fig. 8D). In this PPI network, the top-ranked hub genes in terms of degree are IL1B, CDH1, FOS, AGT, VWF, and others, while the top-ranked hub genes in terms of clustering coefficient include TNNT1, ARC, TXNIP, JUNB, MYBPC2, and others. (Figure 8E and F).

Notably, eight hub genes in the common DE-mRNAs-associated PPI network exhibit potential interactions with NDGR1 (Fig. 9A). Correlation analysis revealed a significant negative correlation between NDRG1 expression in HepG2 cells and HSPA8 and CDH1, as well as a significant positive correlation with ALDOC, ANGPTL4, ANKRD37, CA9, ERBB3 and FOS (Fig. 9B). qRT-qPCR demonstrated that the expression changes of HSPA8, CDH1, ALDOC, ANGPTL4, ANKRD37, CA9, ERBB3, and FOS in each group were consistent with the RNA-seq findings (Fig. 9C; Table 3). These hub genes changed in Huh7 cells in the same way, except for CA9 (Fig. 9D). These findings suggest that NDRG1-mediated ferroptosis in HCC may be achieved by crosstalking among these hub genes.

## Discussion

In the present study, we demonstrate that NDRG1 functions as a tumor-promoting factor with strong predictive value for the prognosis of HCC patients, exerting oncogenic effects by the regulation ferroptosis. NDRG1 has previously been identified as an oncogenic factor in HCC. NDRG1 has been shown to regulate metastasis [7, 28], growth [7, 28], metabolic reprogramming [29], TACE response [30], and drug resistance [31], all of which contribute to the progression of HCC. In contrast to these findings, we observed that NDRG1-mediated processes in HCC are also linked to ferroptosis. In this study, we observed that NDRG1 knockdown accelerated erastin-induced changes in $Fe^{2+}$, total ROS, lipid ROS, and ferroptosis markers (PTGS2, ACSL4, GPX4, SLC7A11, GSH, GSSG) in HepG2 and Huh7 cells. These changes are consistent with the occurrence of ferroptosis [11, 12]. Notably, NDRG1's regulation of ferroptosis is expected to play a role in biological processes. Previous studies have demonstrated that NDRG1 is associated with iron metabolism [32, 33] and lipid metabolism [34], which are

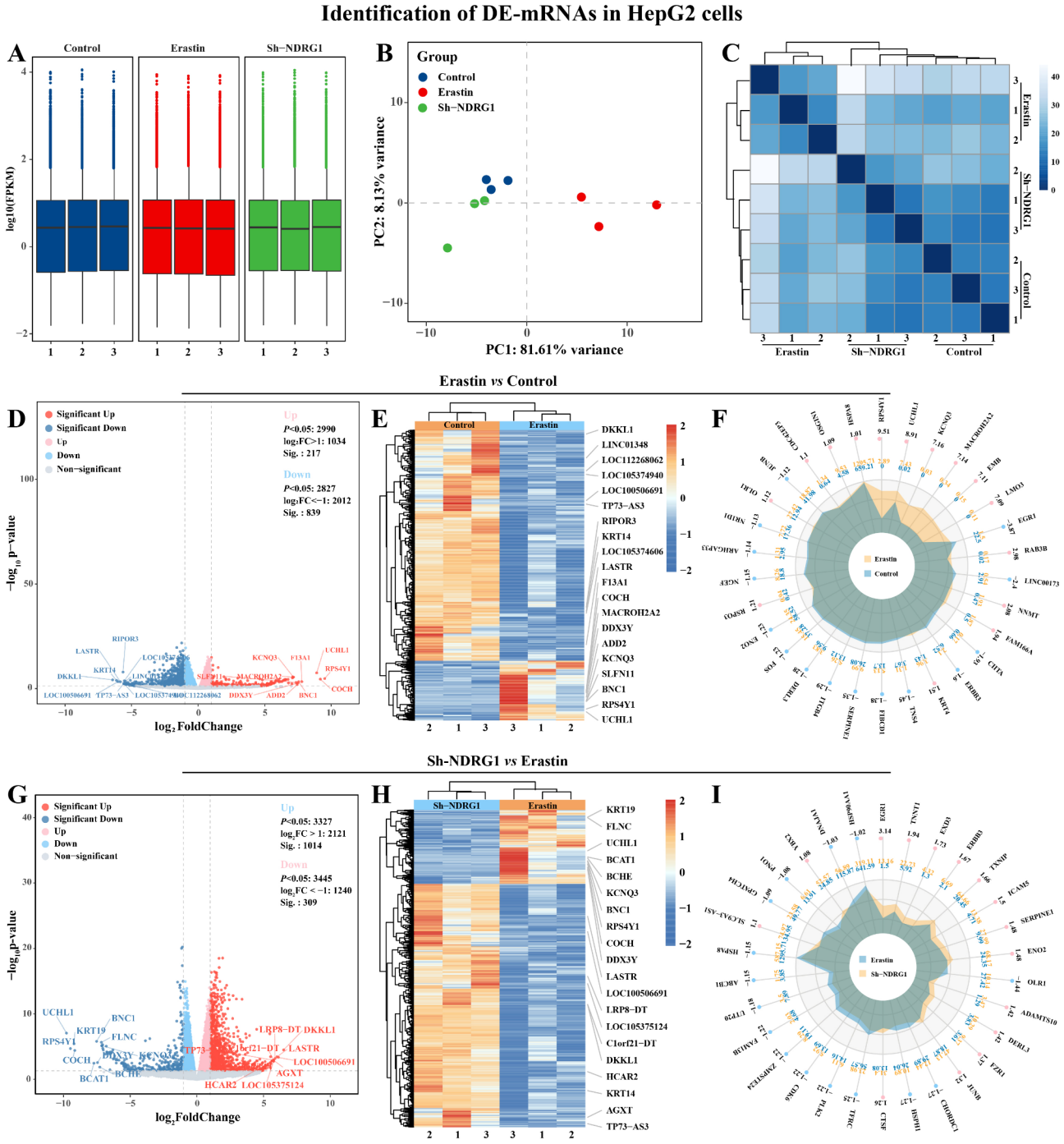


**Fig. 6** Identification of DE-mRNAs in HepG2 cells. **A**: Box plots illustrating the distribution of FPKM data for the calibrated expression profiles of each sample. **B**: PCA showing the differences in expression profiles between and within the Control, Erastin, and Sh-NDRG1 groups. **C**: A distance heatmap displaying the distance between expression profiles obtained using the Euclidean algorithm. Darker colors represent smaller distances and reduced differences. **D** and **G**: Volcano plots demonstrating the distribution of DE-mRNAs (adjusted $P < 0.05$ &$|\log_2 FC| > 1$) in Erastin vs. Control **(D)** and Sh-NDRG1 vs. Erastin **(G)**. **E**and **H**: Expression profiles of DE-mRNAs and clustering of samples based on DE-mRNAs expression in Erastin vs. Control **(E)** and Sh-NDRG1 vs. Erastin **(H)**. **F** and **I**: Radar plots revealing the top 30 DE-mRNAs with|log2FC| in Erastin vs. Control **(F)** and Sh-NDRG1 vs. Erastin **(I)**

critical features of ferroptosis. Moreover, bioinformatics studies have identified NDRG1 as a ferroptosis-related prognostic marker in HCC [9, 10] and melanoma [35]. This aligns with our initial hypothesis and was validated by functional assays in HCC, further refining the understanding of NDRG1's oncogenic mechanism in HCC.

Furthermore, this study elucidates the potential molecular mechanism of NDRG1-mediated ferroptosis

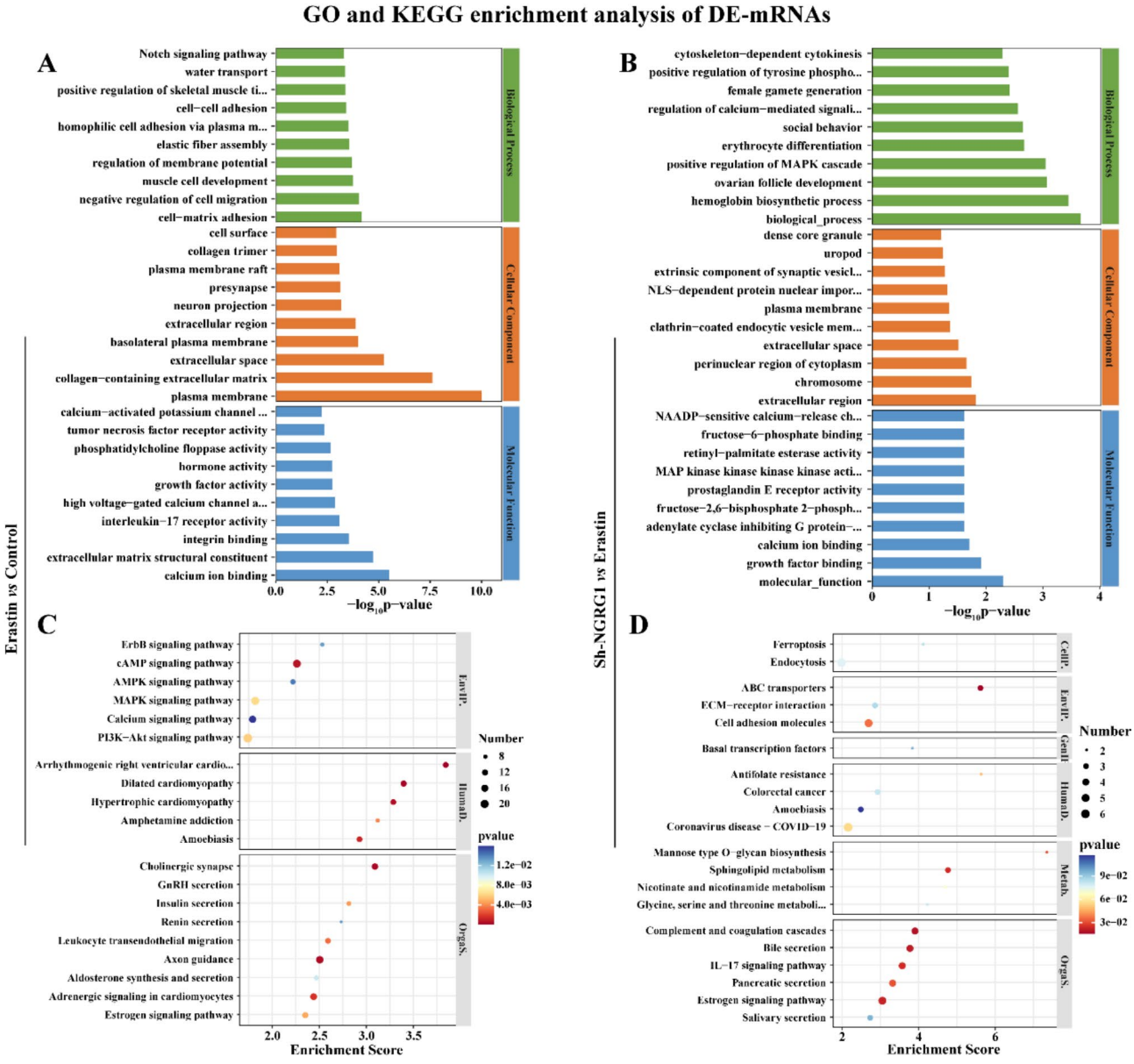


**Fig. 7** GO and KEGG enrichment analysis of DE-mRNAs. **A-B**: GO enrichment analysis identifies biological process (green), cellular component (orange), and molecular function (blue) associated with DE-mRNAs in Erastin vs. Control **(A)** and Sh-NDRG1 vs. Erastin **(B)**. **C-D**: Bubble plots exhibiting the top20 KEGG terms derived from the enrichment analysis of DE-mRNAs in Erastin vs. Control **(C)** and Sh-NDRG1 vs. Erastin **(D)**

through RNA-seq, revealing that DE-mRNAs are predominantly involved in phenotypes such as immunity, growth, metastasis, and ferroptosis, and are associated with the ErbB, cAMP, AMPK, MAPK, and PI3K/AKT pathways. Interestingly, the ErbB [36], cAMP [37], AMPK [38], MAPK [39], and PI3K/AKT [40] pathways were demonstrated to play a role in regulating ferroptosis. These findings suggest that these pathway cascades may also contribute to NDRG1-mediated ferroptosis in HCC. Moreover, this study demonstrates that NDRG1 potentially interacts with eight hub genes, exhibiting significant negative correlations with HSPA8 and CDH1, and significant positive correlations with ALDOC, ANGPTL4, ANKRD37, CA9, ERBB3, and FOS. Notably, with the exception of ANKRD37, seven hub genes have been confirmed to regulate ferroptosis [41–43]. For instance, HBx-induced expression of HSPA8 inhibits ferroptosis and promotes HBV replication, contributing to the development of HBV-associated HCC [41, 42]. CDH1, also referred to E-cadherin, is a protein involved in epithelial-mesenchymal transition in cancer, and its knockdown increases the susceptibility of head and neck cancer cells to ferroptosis [43]. Exosome-derived ANGPTL4 has been shown to inhibit ferroptosis in hypoxic lung cancer [44].

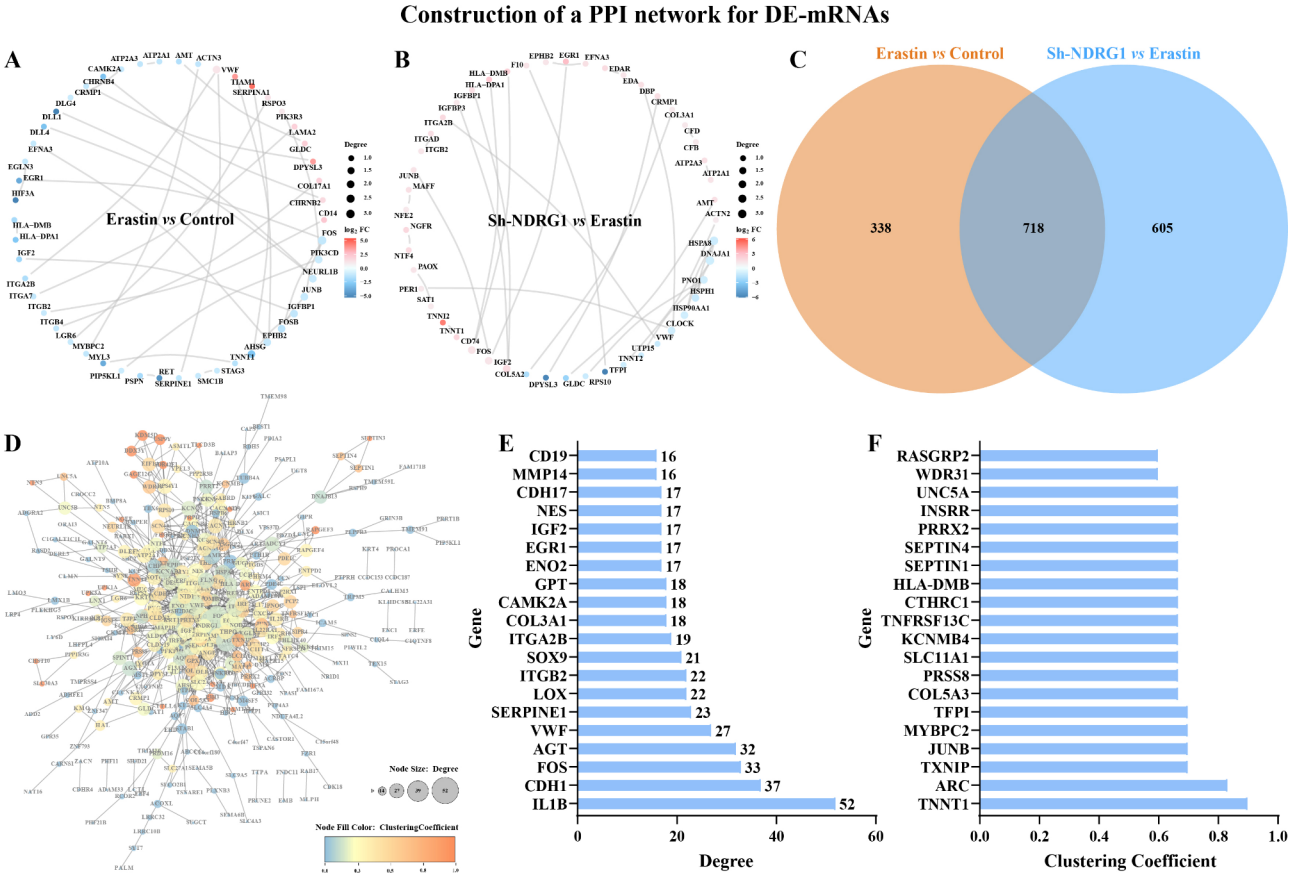


**Fig. 8** Construction of a PPI network for DE-mRNAs. **A-B**: Circled graphs illustrating the PPI network for the top 30 relationship constructed from DE-mRNAs in Erastin vs. Control **(A)** and Sh-NDRG1 vs. Erastin **(B)**. **C**: Common DE-mRNAs in Erastin vs. Control and Sh-NDRG1 vs. Erastin. **D**: PPI networks constructed from common DE-mRNAs. **E-F**: Bar graphs exhibiting hub genes with the top 30 degree **(E)** and clustering coefficient **(F)** in the common DE-mRNAs associated PPI network

These findings suggest that NDRG1-mediated ferroptosis in HCC may be linked to these hub genes. Additionally, the validation results of this study showed that the expression of these hub genes was dysregulated in HCC cells after Erastin treatment, but became more similar to control cells after NDRG1 knockdown. HSPA8 and CDH1 have been demonstrated to inhibit ferroptosis in hepatitis B-associated HCC, anti-tuberculosis drug-induced liver injury, meningioma, and colorectal cancer [42, 45–47]. ANGPTL4 has been shown to promote ferroptosis in sepsis and epithelial ovarian cancer [48, 49]. This study confirmed that NDRG1 knockdown downregulated the expression of HSPA8 and CDH1 and upregulated the level of ANGPTL4 in Erastin-treated HCC cells. Thus, these changes in hub genes are consistent with the way they regulate ferroptosis. Other hub genes may exhibit expression recovery due to compensatory feedback regulation. Moreover, ferroptosis is a dynamic process with distinct phases. Erastin-induced stress likely drives acute transcriptional changes in hub genes, while NDRG1 knockdown may alter the progression or resolution of these phases. The observed "reversion" could reflect a shift in the transcriptional program as cells transition from early stress responses to later adaptive states, rather than a contradiction of NDRG1's role in promoting ferroptosis. Therefore, it is necessary and valuable to further explore the effects of interactions between NDRG1 and these hub genes on ferroptosis.

In conclusion, the present study confirms that NDRG1 acts as an inhibitor of ferroptosis, thereby promoting the progression of HCC. Additionally, HSPA8, CDH1, ALDOC, ANGPTL4, ANKRD37, CA9, ERBB3, and FOS may be potential molecular mechanisms underlying NDRG1-mediated ferroptosis in HCC. However, there are certain limitations to this study that must be addressed. The current study lacks in vivo animal experiments to further investigate the role of NDRG1 in the regulation of ferroptosis. The NDRG1-related molecular mechanisms identified by RNA-seq require further validation of their interactions, as well as functional experiments to explore their role of in HCC ferroptosis. Additionally, knockdown of NDRG1 alone and overexpression of NDRG1 in HCC to explore changes in ferroptosis remain to be further characterized. Our

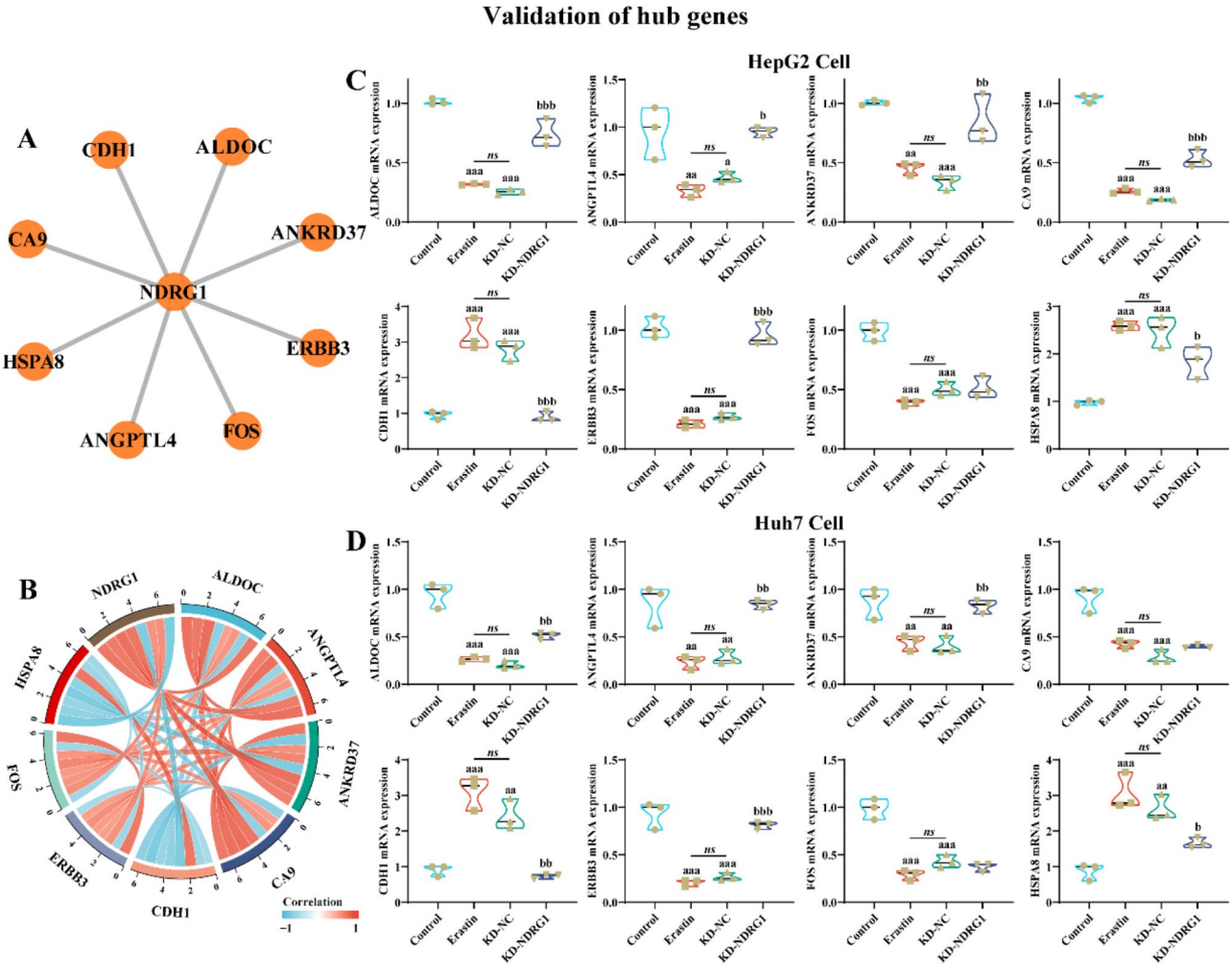


**Fig. 9** Validation of hub genes. **A**: Network diagram illustrating hub genes with potential interactions with NDRG1. **B**: Chordal plots illustrating the expression correlation between NDRG1 and HSPA8, CDH1, ALDOC, ANGPTL4, ANKRD37, CA9, ERBB3, and FOS in RNA-seq expression profiles. **C-D**: Differential expression of HSPA8, CDH1, ALDOC, ANGPTL4, ANKRD37, CA9, ERBB3, and FOS in HepG2 **(C)** and Huh7 **(D)** cells from the Control, Erastin, KD-NC, and KD-NDRG1 groups. Compared to the Control group, $^{a}P<0.05$ and $^{aa}P<0.01$, and $^{aaa}P<0.001$; Compared to the KD-NC group, $^{b}P<0.05$, $^{bb}P<0.01$, and $^{bbb}P<0.001$

**Table 3** Expression of hub genes in RNA-seq

| Gene Id | Erastin vs. Control | | | Sh-NDRG1 vs. Erastin | | |
|---|---|---|---|---|---|---|
| | $log_2FC$ | *p*-value | Regulation | $log_2FC$ | *p*-value | Regulation |
| ALDOC | -1.372 | 5.21E-05 | Down | 1.728 | 1.59E-06 | Up |
| ANGPTL4 | -1.035 | 3.62E-05 | Down | 1.406 | 1.86E-08 | Up |
| ANKRD37 | -1.071 | 5.43E-04 | Down | 1.483 | 9.96E-08 | Up |
| CA9 | -2.192 | 0.0151 | Down | 2.541 | 0.005 | Up |
| CDH1 | 1.384 | 5.35E-04 | Up | -1.634 | 1.79E-04 | Down |
| ERBB3 | -1.605 | 2.68E-20 | Down | 1.674 | 8.03E-18 | Up |
| FOS | -1.234 | 1.73E-22 | Down | 1.272 | 4.52E-15 | Up |
| HSPA8 | 1.009 | 1.45E-15 | Up | -1.148 | 9.60E-21 | Down |

group will address these limitations in the follow-up, which is important for refining the conclusions of this study. Despite these limitations, the findings of this study further refine our understanding of the molecular mechanisms underlying ferroptosis in HCC, offering new insights for future therapeutic strategies targeting ferroptosis-associated HCC.

## Supplementary Information

The online version contains supplementary material available at https://doi.org/10.1186/s12885-025-13954-y.

Supplementary Material 1

Supplementary Material 2: Supplemental File 1. Results of GO enrichment analysis for DE-mRNAs in Erastin vs. Control and Sh-NDRG1 vs. Erastin.

Supplementary Material 3: Supplemental File 2. Results of KEGG enrichment analysis for DE-mRNAs in Erastin vs. Control and Sh-NDRG1 vs. Erastin.

**Author contributions**
L.L., T.W., G.G., B.L., J.F., L.X., H.Z., and X. G. conceived and designed the experiments; L.L., T.W., G.G., B.L., J.F., L.X., H.Z., and X. G. performed the experiments; L.L. and T.W. analyzed and interpreted the data; G.G. and B.L. contributed reagents/materials/analysis tools; L.L. wrote original draft; T.W., G.G., B.L., J.F., L.X., H.Z., and X. G. reviewed and edited draft. All authors have read and agreed to the published version of the manuscript.

**Funding**
Scientific Research Fund of Yunnan Provincial Department of Education (grant No. 2023J0937).

**Data availability**
The data that support the findings of this study are available on request from the corresponding author, upon reasonable request.

## Declarations

**Ethical approval**
Ethics Committee of the People's Hospital of Lincang approved this study (Approval Number: 2023-30), and all protocol was conducted in strict accordance with the Declaration of Helsinki.

**Consent for publication**
All subjects signed an informed consent form and agreed to publication.

**Competing interests**
The authors declare no competing interests.

Received: 17 July 2024 / Accepted: 17 March 2025
Published online: 21 March 2025

**References**

1. Sung H, Ferlay J, Siegel RL, et al. Global cancer statistics 2020: GLOBOCAN estimates of incidence and mortality worldwide for 36 cancers in 185 Countries[J]. CA Cancer J Clin. 2021;71(3):209–49.
2. Liu D, Song T. Changes in and challenges regarding the surgical treatment of hepatocellular carcinoma in China[J]. Biosci Trends. 2021;15(3):142–7.
3. Zhou H, Song T. Conversion therapy and maintenance therapy for primary hepatocellular carcinoma[J]. Biosci Trends. 2021;15(3):155–60.
4. Ellen TP, Ke Q, Zhang P, et al. NDRG1, a growth and cancer related gene: regulation of gene expression and function in normal and disease states[J]. Carcinogenesis. 2008;29(1):2–8.
5. Joshi V, Lakhani SR, Mccart Reed AE. NDRG1 in cancer: A suppressor, promoter, or Both?[J]. Cancers (Basel). 2022; 14(23).
6. Bae DH, Jansson PJ, Huang ML, et al. The role of NDRG1 in the pathology and potential treatment of human cancers[J]. J Clin Pathol. 2013;66(11):911–7.
7. Dang H, Chen L, Tang P, et al. LINC01419 promotes cell proliferation and metastasis in hepatocellular carcinoma by enhancing NDRG1 promoter activity[J]. Cell Oncol (Dordr). 2020;43(5):931–47.
8. Cheng Q, Ning S, Zhu L, et al. NDRG1 facilitates self-renewal of liver cancer stem cells by preventing EpCAM ubiquitination[J]. Br J Cancer. 2023;129(2):237–48.
9. Han F, Cao D, Zhu X, et al. Construction and validation of a prognostic model for hepatocellular carcinoma: inflammatory ferroptosis and mitochondrial metabolism indicate a poor prognosis[J]. Front Oncol. 2022;12:972434.
10. Du X, Zhang Y. Integrated analysis of Immunity- and Ferroptosis-Related biomarker signatures to improve the prognosis prediction of hepatocellular Carcinoma[J]. Front Genet. 2020;11:614888.
11. Zhao L, Zhou X, Xie F, et al. Ferroptosis in cancer and cancer immunotherapy[J]. Cancer Commun (Lond). 2022;42(2):88–116.
12. Liang D, Minikes AM, Jiang X. Ferroptosis at the intersection of lipid metabolism and cellular signaling[J]. Mol Cell. 2022;82(12):2215–27.
13. Zhao S, Zheng W, Yu C, et al. The role of ferroptosis in the treatment and drug resistance of hepatocellular Carcinoma[J]. Front Cell Dev Biol. 2022;10:845232.
14. Huang Z, Xia H, Cui Y, et al. Ferroptosis: from basic research to clinical therapeutics in hepatocellular Carcinoma[J]. J Clin Transl Hepatol. 2023;11(1):207–18.
15. Pan F, Lin X, Hao L, et al. The critical role of ferroptosis in hepatocellular Carcinoma[J]. Front Cell Dev Biol. 2022;10:882571.
16. Park SJ, Yoon BH, Kim SK, et al. GENT2: an updated gene expression database for normal and tumor tissues[J]. BMC Med Genomics. 2019;12(Suppl 5):101.
17. Tang Z, Kang B, Li C, et al. GEPIA2: an enhanced web server for large-scale expression profiling and interactive analysis[J]. Nucleic Acids Res. 2019;47(W1):W556–60.
18. Lin H, Zelterman DJT. Model Survival Data: Extending Cox Model[J]. 2002;44:85–6.
19. Eng KH, Schiller E, Morrell K. On representing the prognostic value of continuous gene expression biomarkers with the restricted mean survival curve[J]. Oncotarget. 2015;6(34):36308–18.
20. Yao F, Deng Y, Zhao Y, et al. A targetable LIFR-NF-κB-LCN2 axis controls liver tumorigenesis and vulnerability to ferroptosis[J]. Nat Commun. 2021;12(1):7333.
21. Love MI, Huber W, Anders S. Moderated Estimation of fold change and dispersion for RNA-seq data with DESeq2[J]. Genome Biol. 2014;15(12):550.
22. Wu T, Hu E, Xu S, et al. ClusterProfiler 4.0: A universal enrichment tool for interpreting omics data[J]. Innov (Camb). 2021;2(3):100141.
23. Ginestet C. J Royal Stat Soc Ser A: Stat Soc. 2011;174(1):245–6. ggplot2: Elegant Graphics for Data Analysis[J].
24. Szklarczyk D, Gable AL, Lyon D, et al. STRING v11: protein-protein association networks with increased coverage, supporting functional discovery in genome-wide experimental datasets[J]. Nucleic Acids Res. 2019;47(D1):D607–13.
25. Otasek D, Morris JH, Bouças J, et al. Cytoscape automation: empowering workflow-based network analysis[J]. Genome Biol. 2019;20(1):185.
26. Kontoghiorghes GJ. New iron metabolic pathways and chelation targeting strategies affecting the treatment of all types and stages of Cancer[J]. Int J Mol Sci. 2022; 23(22).
27. Macías-Rodríguez RU, Inzaugarat ME, Ruiz-Margáin A et al. Reclassifying hepatic cell death during liver damage: Ferroptosis-A novel form of Non-Apoptotic cell death?[J]. Int J Mol Sci. 2020; 21(5).
28. Zhou W, Huang K, Zhang Q, et al. LINC00844 promotes proliferation and migration of hepatocellular carcinoma by regulating NDRG1 expression[J]. PeerJ. 2020;8:e8394.
29. Guo DD, Xie KF, Luo XJ. Hypoxia-induced elevated NDRG1 mediates apoptosis through reprograming mitochondrial fission in HCC[J]. Gene. 2020;741:144552.
30. Tang B, Wang Y, Zhu J, et al. TACE responser NDRG1 acts as a guardian against ferroptosis to drive tumorgenesis and metastasis in HCC[J]. Biol Proced Online. 2023;25(1):13.
31. Jung EU, Yoon JH, Lee YJ, et al. Hypoxia and retinoic acid-inducible NDRG1 expression is responsible for doxorubicin and retinoic acid resistance in hepatocellular carcinoma cells[J]. Cancer Lett. 2010;298(1):9–15.
32. Le NT, Richardson DR. Iron chelators with high antiproliferative activity up-regulate the expression of a growth inhibitory and metastasis suppressor gene: a link between iron metabolism and proliferation[J]. Blood. 2004;104(9):2967–75.
33. Whitnall M, Howard J, Ponka P, et al. A class of iron chelators with a wide spectrum of potent antitumor activity that overcomes resistance to chemotherapeutics[J]. Proc Natl Acad Sci U S A. 2006;103(40):14901–6.
34. Sevinsky CJ, Khan F, Kokabee L, et al. NDRG1 regulates neutral lipid metabolism in breast cancer cells[J]. Breast Cancer Res. 2018;20(1):55.
35. Gao Y, Hou Q, Guo R, et al. Effect of sun exposure-induced ferroptosis mechanisms on pathology and potential biological processes of primary melanoma by microarray data analysis[J]. Front Genet. 2022;13:998792.
36. Zhao X, Zhang J, Zhang W, et al. A chiral fluorescent Ir(iii) complex that targets the GPX4 and erbb pathways to induce cellular ferroptosis[J]. Chem Sci. 2023;14(5):1114–22.

37. Guan Q, Wang Z, Hu K, et al. Melatonin ameliorates hepatic ferroptosis in NAFLD by inhibiting ER stress via the MT2/cAMP/PKA/IRE1 signaling Pathway[J]. Int J Biol Sci. 2023;19(12):3937–50.
38. Lee H, Zandkarimi F, Zhang Y, et al. Energy-stress-mediated AMPK activation inhibits ferroptosis[J]. Nat Cell Biol. 2020;22(2):225–34.
39. Wang X, Zhang C, Zou N, et al. Lipocalin-2 Silencing suppresses inflammation and oxidative stress of acute respiratory distress syndrome by ferroptosis via Inhibition of MAPK/ERK pathway in neonatal mice[J]. Bioengineered. 2022;13(1):508–20.
40. Yi J, Zhu J, Wu J, et al. Oncogenic activation of PI3K-AKT-mTOR signaling suppresses ferroptosis via SREBP-mediated lipogenesis[J]. Proc Natl Acad Sci U S A. 2020;117(49):31189–97.
41. Wang Y, Zhao M, Zhao L, et al. HBx-Induced HSPA8 stimulates HBV replication and suppresses ferroptosis to support liver cancer Progression[J]. Cancer Res. 2023;83(7):1048–61.
42. Deng W, Ai J, Zhang W, et al. Arginine methylation of HSPA8 by PRMT9 inhibits ferroptosis to accelerate hepatitis B virus-associated hepatocellular carcinoma progression[J]. J Transl Med. 2023;21(1):625.
43. Lee J, You JH, Kim MS, et al. Epigenetic reprogramming of epithelial-mesenchymal transition promotes ferroptosis of head and neck cancer[J]. Redox Biol. 2020;37:101697.
44. Zhang Y, Liu X, Zeng L, et al. Exosomal protein angiopoietin-like 4 mediated radioresistance of lung cancer by inhibiting ferroptosis under hypoxic microenvironment[J]. Br J Cancer. 2022;127(10):1760–72.
45. Zhou J, Tan Y, Hu L, et al. Inhibition of HSPA8 by rifampicin contributes to ferroptosis via enhancing autophagy[J]. Liver Int. 2022;42(12):2889–99.
46. Bao Z, Hua L, Ye Y, et al. MEF2C Silencing downregulates NF2 and E-cadherin and enhances Erastin-induced ferroptosis in meningioma[J]. Neuro Oncol. 2021;23(12):2014–27.
47. Li B, Wei Z, Wang Z, et al. Fusobacterium nucleatum induces oxaliplatin resistance by inhibiting ferroptosis through E-cadherin/β-catenin/GPX4 axis in colorectal cancer[J]. Free Radic Biol Med. 2024;220:125–38.
48. Yang WH, Huang Z, Wu J, et al. A TAZ-ANGPTL4-NOX2 axis regulates ferroptotic cell death and chemoresistance in epithelial ovarian Cancer[J]. Mol Cancer Res. 2020;18(1):79–90.
49. Deng W, Zhong L, Ye S, et al. Mir22hg facilitates ferritinophagy-mediated ferroptosis in sepsis by recruiting the m6A reader YTHDC1 and enhancing Angptl4 mRNA stability[J]. J Bioenerg Biomembr. 2024;56(4):405–18.

## Publisher's note